The March 2022

Giovanni News

The 2022 Giovanni Image Hall of Fame

Welcome to the special issue of *The Giovanni News* newsletter featuring the new members of the Giovanni Image Hall of Fame!

As the pace of Giovanni development has slowed over the past years, we have not been publishing new issues of *The Giovanni News*. The NASA Goddard Earth Sciences Data and Information Services Center (GES DISC) is conducting a multitude of activities devoted to making it easier to access, acquire, and analyze the Earth science data that are in its archive. In the future, *The Giovanni News* newsletter may be replaced with a GES DISC newsletter covering all of these different activities.

This is also the first new selection of Giovanni Image Hall of Fame images since 2019, so there were numerous candidates to examine. The final list of candidate images exceeded 60. This list was reduced to the 15 images that are described and presented here.

As with previous Hall of Fame "inductions", a certificate will be emailed to the contact author of each paper in which the image appeared.

We hope and expect that the images will provide interesting perspectives on how the data which Giovanni provides can be used, the skill and creativity of the researchers who use them, and the remarkable variety of scientific topics that can be examined with data from the NASA GES DISC.

The 2022 Giovanni Image Hall of Fame

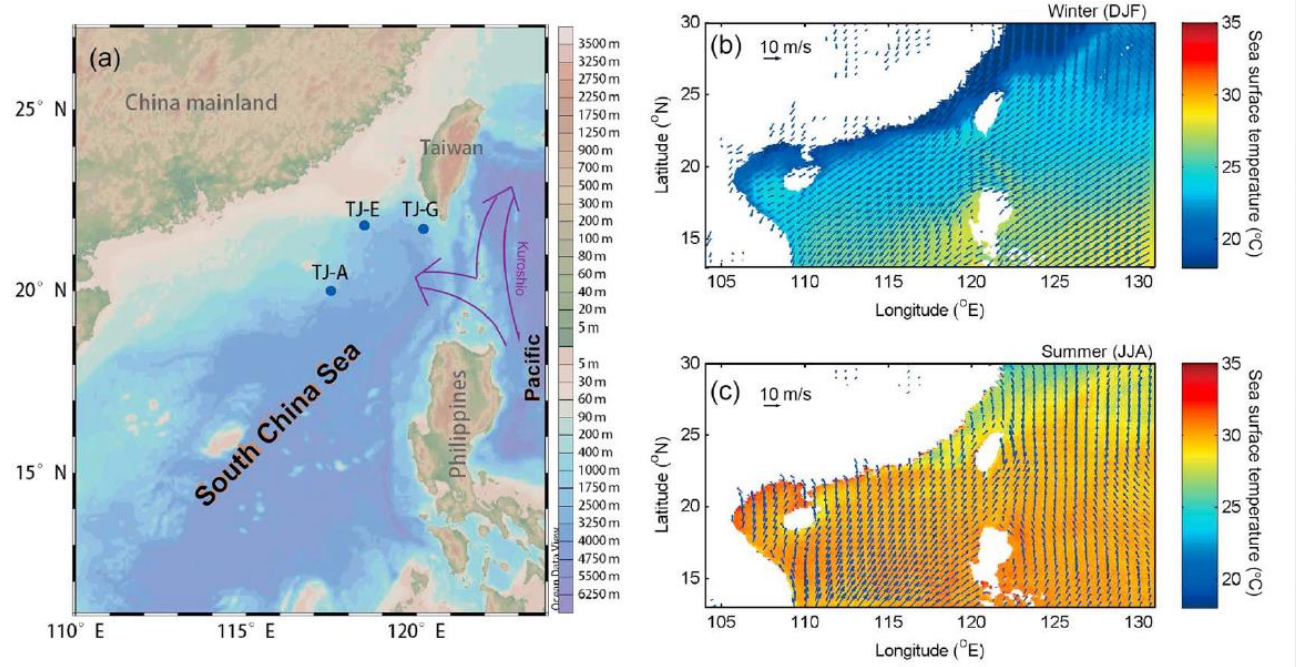

Figure 1. Map showing the mooring sites of TJ-A, TJ-E, and TJ-E in the northern South China Sea (a). The map was plotted by Ocean Data View (Schlitzer, 2018), and the seasonal average sea surface temperature (MODISA_L3m) in winter (a) and summer (b; from December 2013 to February 2015) is superimposed on wind speed (blue arrows, MERRA-2 model at 1,000 hPa); both the temperature and wind speed data were retrieved from https://giovanni.gsfc.nasa.gov/giovanni.

Description

The figure from Jin et al. (2019) provides climatological context for their investigation of coccolithophore biology in the South China Sea. The sea surface temperature data are from the Moderate Resolution Imaging Spectroradiometer on the Aqua satellite (MODIS-Aqua), and the windspeed data are from the Modern-Era Retrospective analysis for Research and Applications – 2 (MERRA-2) dataset, archived at the NASA GES DISC.

Citation

Jin, X. B., Liu, C. L., Zhao, Y. L., Zhang, Y. W., Wen, K., Lin, S., et al. (2019) **Two production stages of coccolithophores in winter as revealed by sediment traps in the northern South China Sea**. *Journal of Geophysical Research: Biogeosciences*, 124, 16 pages, doi:10.1029/2019JG005070.

The 2022 Giovanni Image Hall of Fame

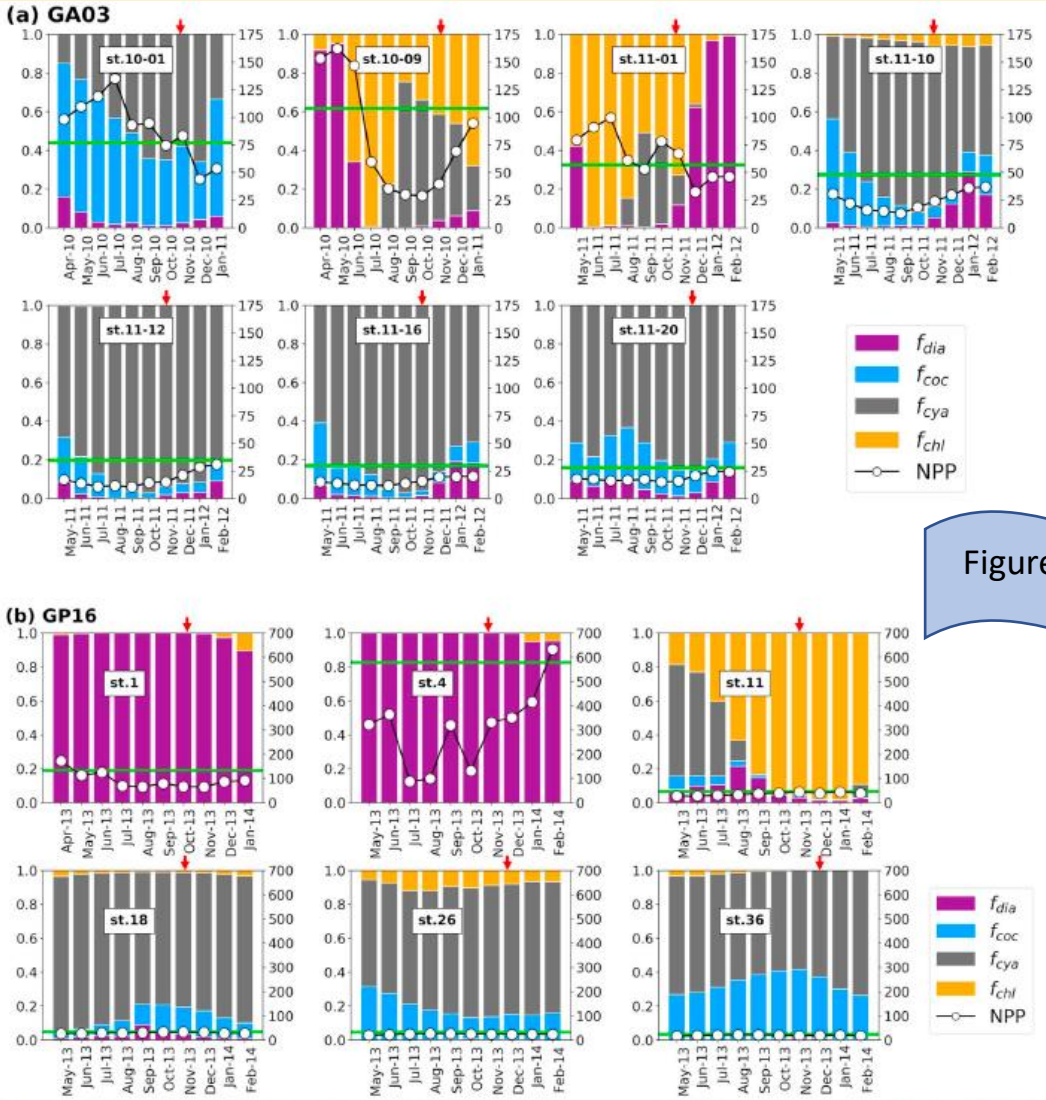

Figure of Special Merit

Fig. 5. Times-series satellite-based monthly average fraction (no unit, left Y axis) of diatoms (f_{dia}), coccolithophores (f_{coc}), cyanobacteria (f_{cya}), and chlorophytes (f_{chl}) with monthly net primary production (mmol C m^{-2} d^{-1}, right Y axis) along the (a) GA03, (b) GP16, and (c) GA01 transects. The red arrow denotes the sampling time at each station. The horizontal green line denotes 130% of winter average NPP value, which we used to define the existence of a bloom. Phytoplankton data are from the Giovanni online data system https://giovanni.gsfc.nasa.gov/giovanni/. Net primary production (NPP) data are from http://www.science.oregonstate.edu/ocean.productivity/. Note that the NPP scale differs among transects.

Description

This noteworthy figure from Tang and Stewart (2019) depicts phytoplankton group predominance and annual variability based on data from the NASA Ocean Biogeochemical Model (NOBM) available in Giovanni. The data are shown are net primary productivity data for stations on three research cruise transects. (Part c is not shown.)

Citation

Tang, Y., and Stewart, G. (2019) **The 210Po/210Pb method to calculate particle export: Lessons learned from the results of three GEOTRACES transects**. *Marine Chemistry*, 217, 16 pages, doi: 10.1016/j.marchem.2019.103692.

The 2022 Giovanni Image Hall of Fame

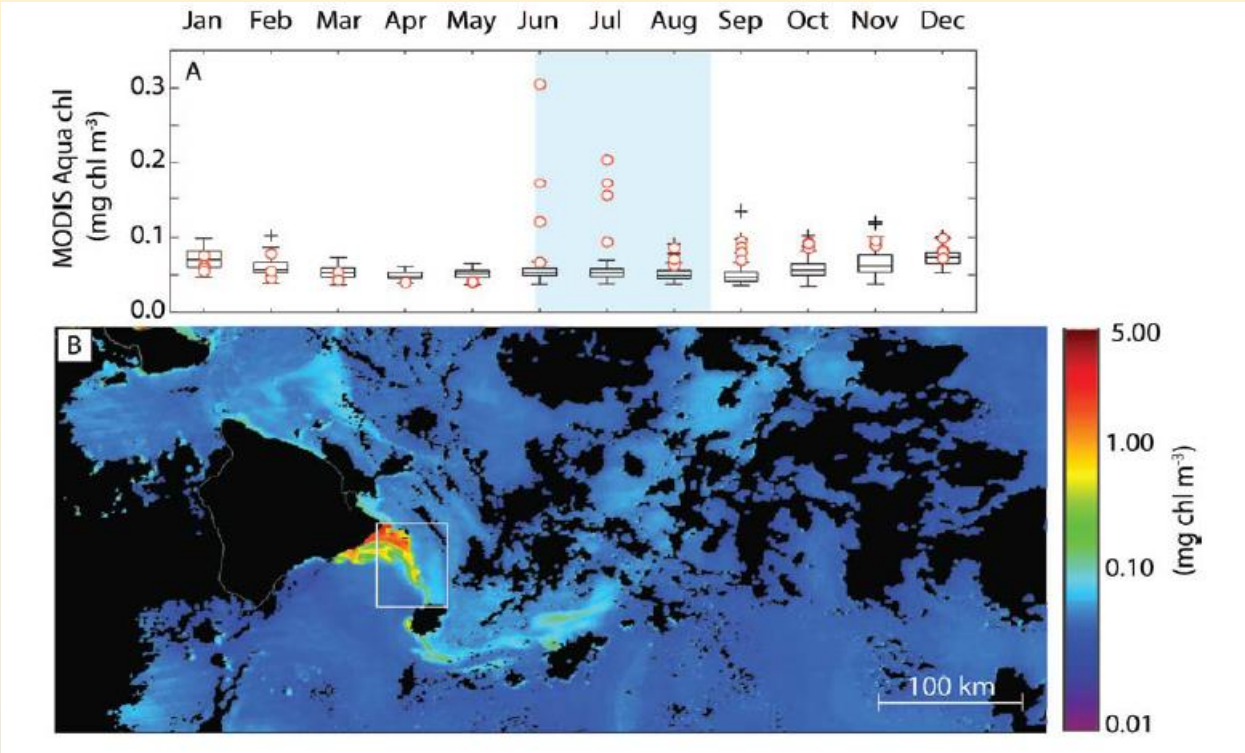

Description

The image and figure from Wilson et al. (2019) show the phytoplankton bloom activity that was triggered by the flank eruption and ocean-entering lava flows from Hawaii's Kilauea volcano in May-June 2018. The voluminous lava flows submerged and descended on the island flanks, and the heat of the lava caused deep waters with increased nutrient concentrations to rise to the surface, enhancing phytoplankton productivity. The time-series of MODIS-Aqua chlorophyll was created in Giovanni with data provided by the Ocean Biology Distributed Active Archive Center (OBDAAC).

Citation

Wilson, S.T., Hawco, N.J., Armbrust, E.V., Barone, B., Björkman, K.M., Boysen, A.K., Burgos, M., Burrell, T.J., Casey, J.R., DeLong, E.F. Dugenne, M., Dutkiewicz, S., Dyhrman, S.T., Ferrón, S., Follows, M.J., Foreman, R.K., Funkey, C.P., Harke, M.J., Henke, B.A., Hill, C.N., Hynes, A.M., Ingalls, A.E., Jahn, O., Kelly, R.L.,Knapp, A.M., Letelier, R.M., Ribalet, F., Shimabukuro, E.M., Tabata, R.K.S., Turk-Kubo, K.A., White, A.E., Zehr, J.P., John, S., and Karl, D.M. (2019) **Kīlauea lava fuels phytoplankton bloom in the North Pacific Ocean**. *Science*, 365(6457), 1040-1044, doi:10.1126/science.aax4767.

The 2022 Giovanni Image Hall of Fame

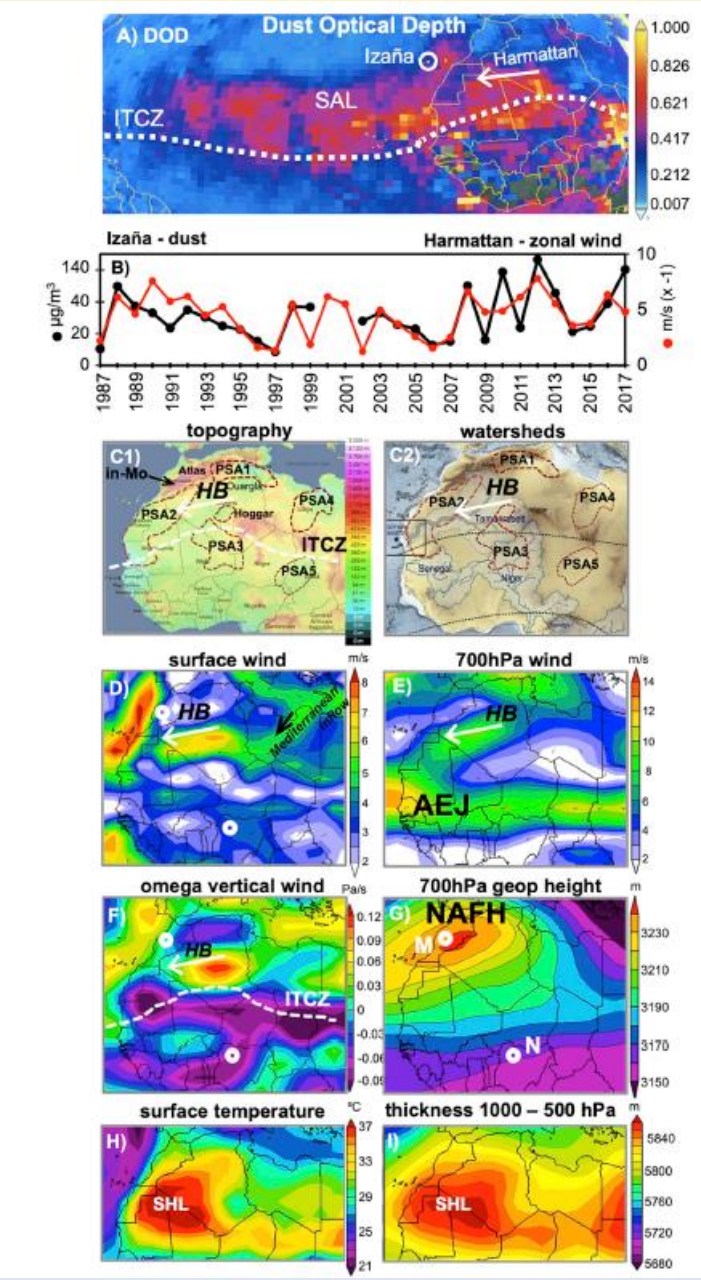

Description

Figure 2 from Rodriguez et al. (2019) combines dust (aerosol) optical depth from MODIS-Aqua, mapped with Giovanni, with a variety of other data variables that allow examination of a Saharan dust outbreak in August 2010. Pressure, temperature, and wind fields provide a multi-faceted view of this event. The time-series in panel B is based on weather station data. The figure shows how data and graphics from Giovanni provide important context for event analysis.

Citation

Rodríguez, S., Calzolai, G., Chiari, M., Nava, S., García, M.I., López-Solano, J., Marrero, C., López-Darias, J., Cuevas, E., Alonso-Pérez, S., Prats, N., Amato, F. Lucarelli, F., and Querol, X. (2019) **Rapid changes of dust geochemistry in the Saharan Air Layer linked to sources and meteorology.** *Atmospheric Environment*, 17 pages, doi:10.1016/j.atmosenv.2019.117186.

The 2022 Giovanni Image Hall of Fame

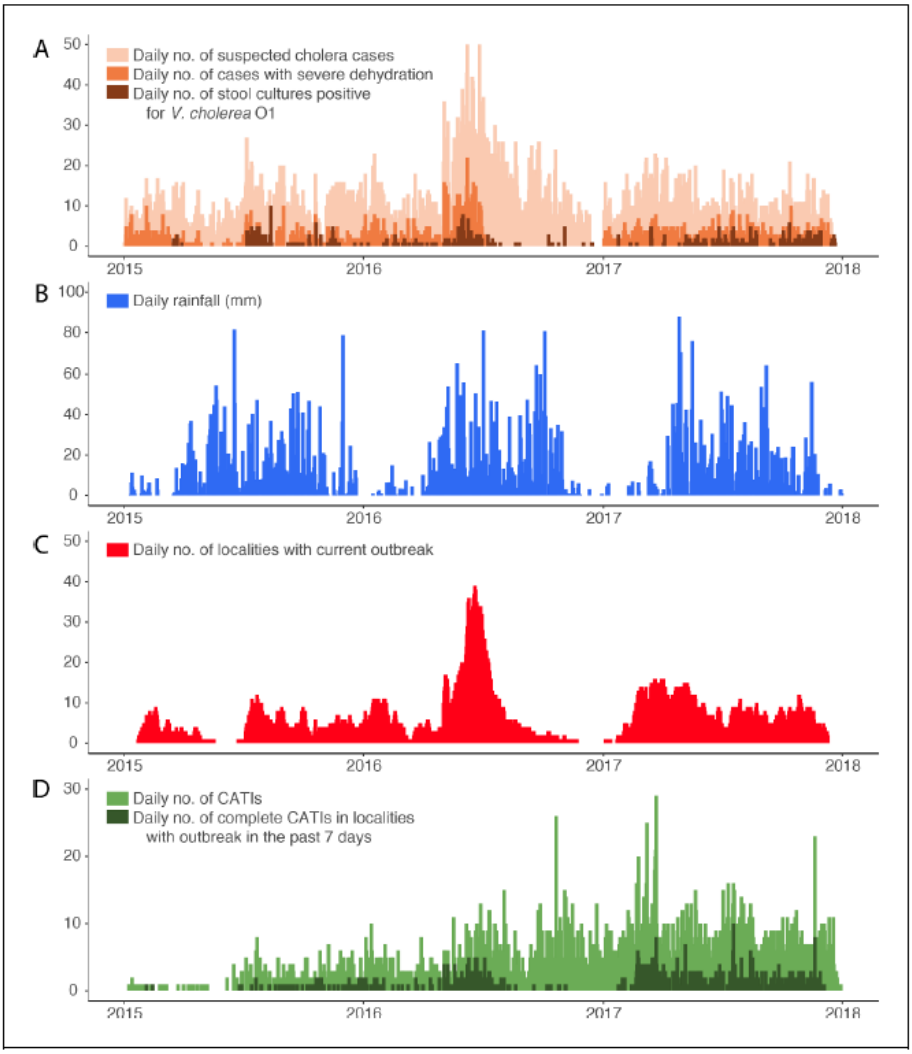

Figure 1. Daily evolution of (**A**) suspected cholera cases, cases with severe dehydration and stool cultures positive for *V. cholerae* O1, (**B**) accumulated rainfall, (**C**) localities with a current cholera outbreak, and (**D**) case-area targeted interventions (CATIs), in the Centre department of Haiti between January 2015 and December 2017.

Description

The use of NASA Earth science data for public health applications has been increasing every year. Because cholera is a waterborne disease, precipitation data from the GES DISC in Giovanni have been commonly used for research on this disease. The figure from Michel et al. (2019) combines daily precipitation data (panel B) with case numbers, locations, and interventions in Haiti.

Citation

Michel, E., Gaudart, J., Beaulieu, S., Bulit, G., Piarroux, M., Boncy, J., Dely, P., Piarroux, R. and Rebaudet, S. (2019) **Estimating effectiveness of case-area targeted response interventions against cholera in Haiti**. *eLife*, 8, 34 pages, doi:10.7554/eLife.50243.

The 2022 Giovanni Image Hall of Fame

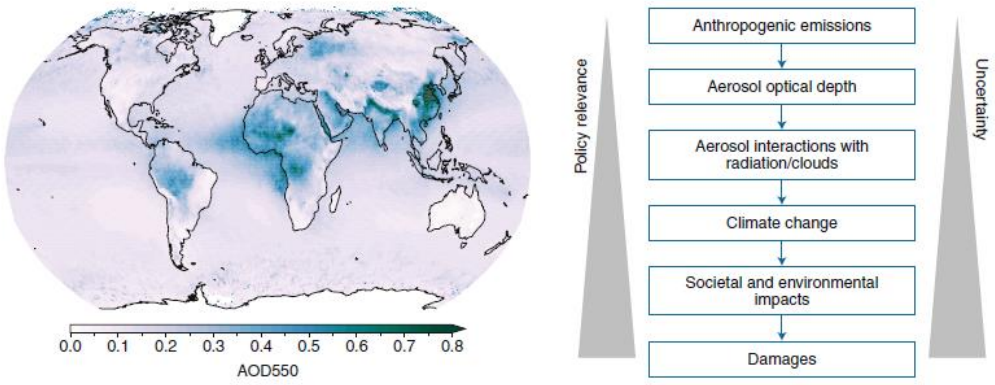

Fig. 1 | Anthropogenic aerosols in the climate system. Annual mean aerosol optical depth at 550 nm (AOD550) for 2010, from the satellite instrument MODIS-Aqua (left); and a schematic illustration of the cause-and-effect chain relating emissions to damages (right). Anthropogenic aerosols like those shown on the left interact with clouds and radiation to cause net surface cooling, and tracing the ultimate economic impacts of emissions can be an uncertain exercise but is highly policy-relevant, as illustrated in the schematic. Zheng and colleagues[2] estimate that aerosol-induced cooling has economically benefited developing countries in warmer climates and harmed high-latitude developed countries. This implies that aerosol emissions have partially offset the increases to economic inequality that would have occurred in their absence. Left panel, data from NASA Giovanni database (https://giovanni.gsfc.nasa.gov/giovanni/); right panel adapted from ref. [7].

Description

An increasing area of public health and economic concern around the world is air quality, and surprising consequences can be discerned from the patterns of global air quality. This figure from an article in *Nature Climate Change* shows worldwide aerosol optical depth (AOD) from MODIS-Aqua, mapped with Giovanni, and a schematic diagram illustrating the conclusions described in the article. The surprising result described here is that cooling from increased aerosol concentrations has provided an economic *benefit* to *developing* countries in warmer regions of the world, but cooler conditions have actually been an economic *detriment* to *developed* countries located at higher latitudes.

Citation

Lund, M.T. (2020) **Dirty air offsets inequality**. *Nature Climate Change* 10, 185–186, doi:10.1038/s41558-020-0714-3.

The 2022 Giovanni Image Hall of Fame

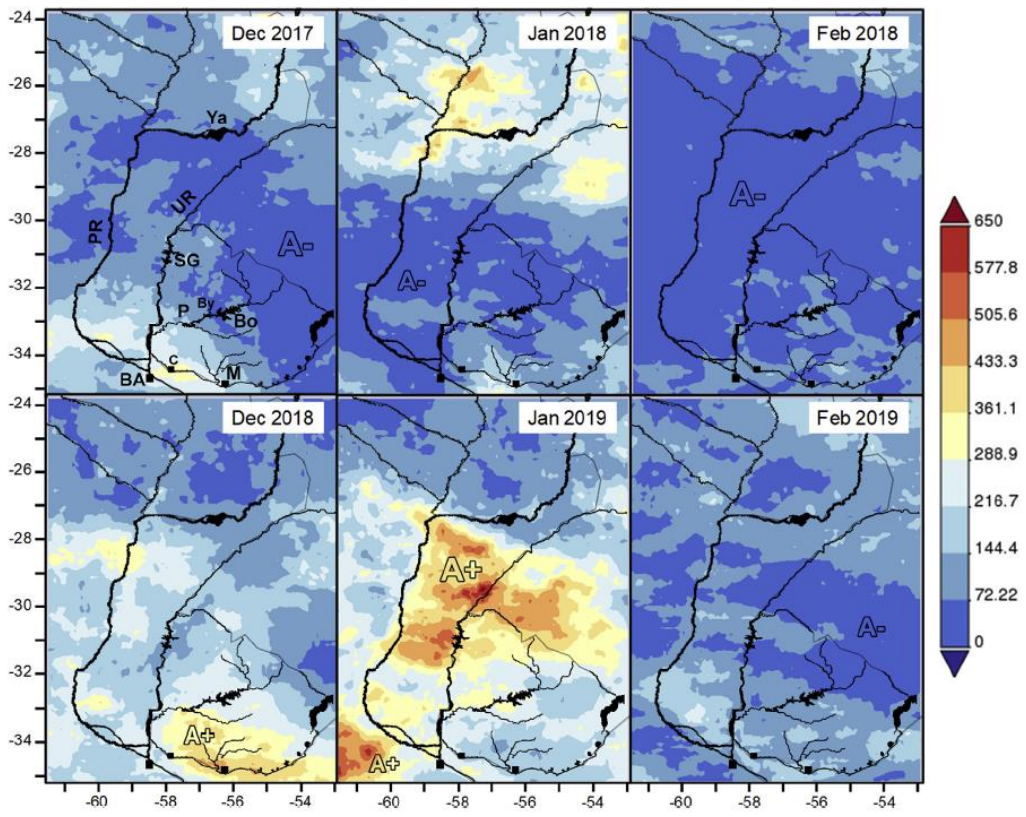

Fig. 2. Total monthly precipitation estimate (mm month^{-1}) (combined microwave-IR) - Late Run daily 0.1 deg. [GPM GPM_3IMERGDL v06]. Letters in the upper left map indicate: PR, Paraná River; UR, Uruguay River; Ya, Yacyretá reservoir; SG, Salto Grande reservoir; P, Palmar reservoir; By: Baygorria reservoir; Bo, Bonete reservoir; BA, Buenos Aires city; C: Colonia city; M, Montevideo city. Black squares indicate the location of the main cities on the Rio de la Plata coast. A+ and A-denote positive and negative precipitation anomalies, respectively.

Description

Along with air quality, water quality is another important area of application for NASA remotely-sensed data. NASA data can be used to research the causes of adverse water quality conditions. In this study of a cyanobacterial bloom in Argentina's Rio de la Plata estuary, Integrated Multi-satellitE Retrievals for GPM (IMERG) data in Giovanni clearly show heavy rains that induced runoff and high nutrient concentrations in the estuary, conditions which encouraged the proliferation of the bloom. (GPM stands for Global Precipitation Measurement.)

Citation

Aubriot, L., Zabaleta, B., Bordet, F., Sienra, D., Risso, J., Achkar, M. and Somma, A. (2020) **Assessing the origin of a massive cyanobacterial bloom in the Río de la Plata (2019): Towards an early warning system**. *Water Research*, 15 pages, doi:10.1016/j.watres.2020.115944.

The 2022 Giovanni Image Hall of Fame

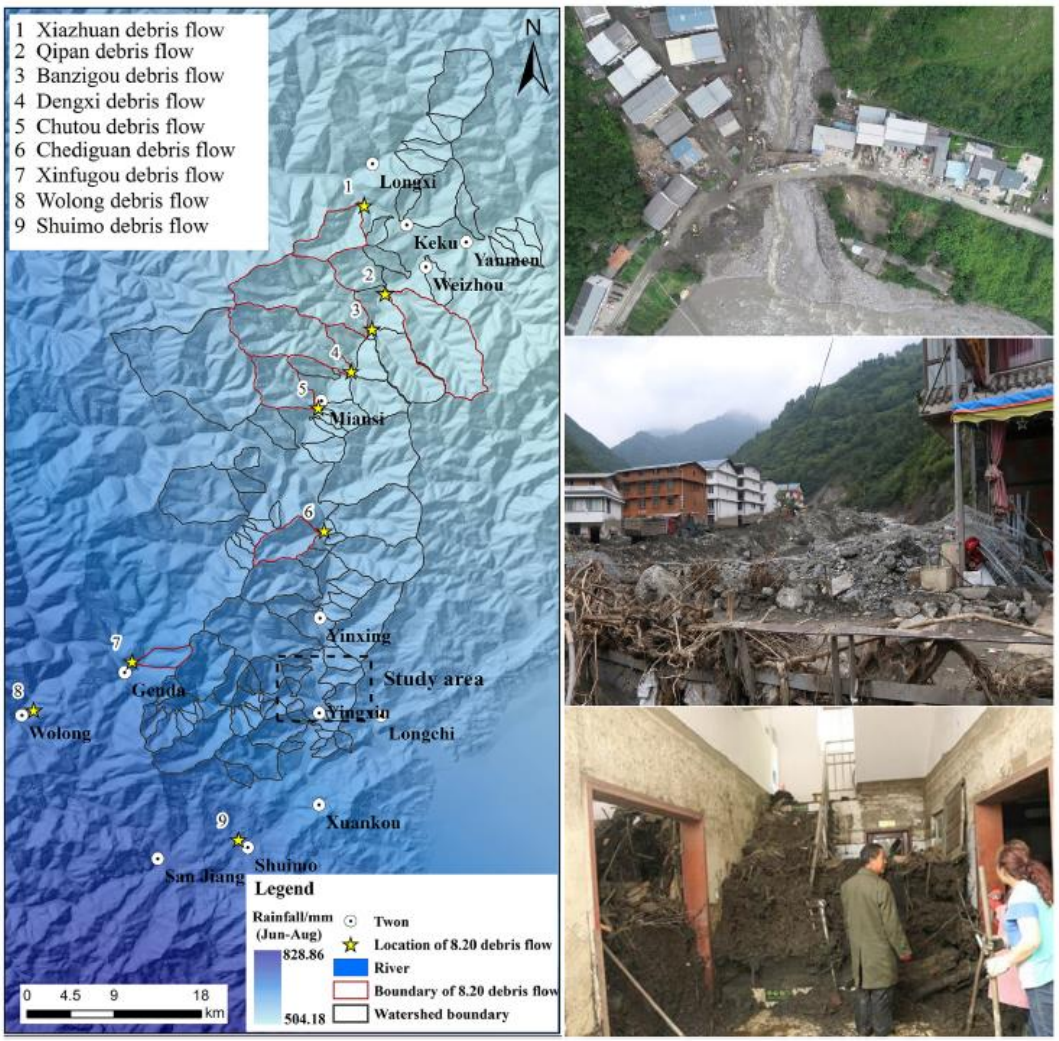

Fig. 16. Distribution of debris flows (left) and damage examples of the Wolong debris flow (right) on August 20, 2019 (resource of rainfall data: https://giovanni.gsfc.nasa.gov/giovanni/).

Description

Data in Giovanni can be used in remarkable ways. In this study of landslides in the region of the 2008 Wenchuan earthquake in China, the average summer (June-August) amount of precipitation in the region was acquired from Giovanni and plotted as shades of blue overlying the topographic location map shown at left. The map also shows the locations of landslides and the mountainous character of the region.

Citation

Chen, M., Tang, C., Xiong, J., Shi, Q.Y., Li, N., Gong, L.F., Wang, X.D., and Tie, Y. (2020) **The long-term evolution of landslide activity near the epicentral area of the 2008 Wenchuan earthquake in China**. *Geomorphology*, 17 pages, doi:10.1016/j.geomorph.2020.107317.

The 2022 Giovanni Image Hall of Fame

Figure of Special Merit

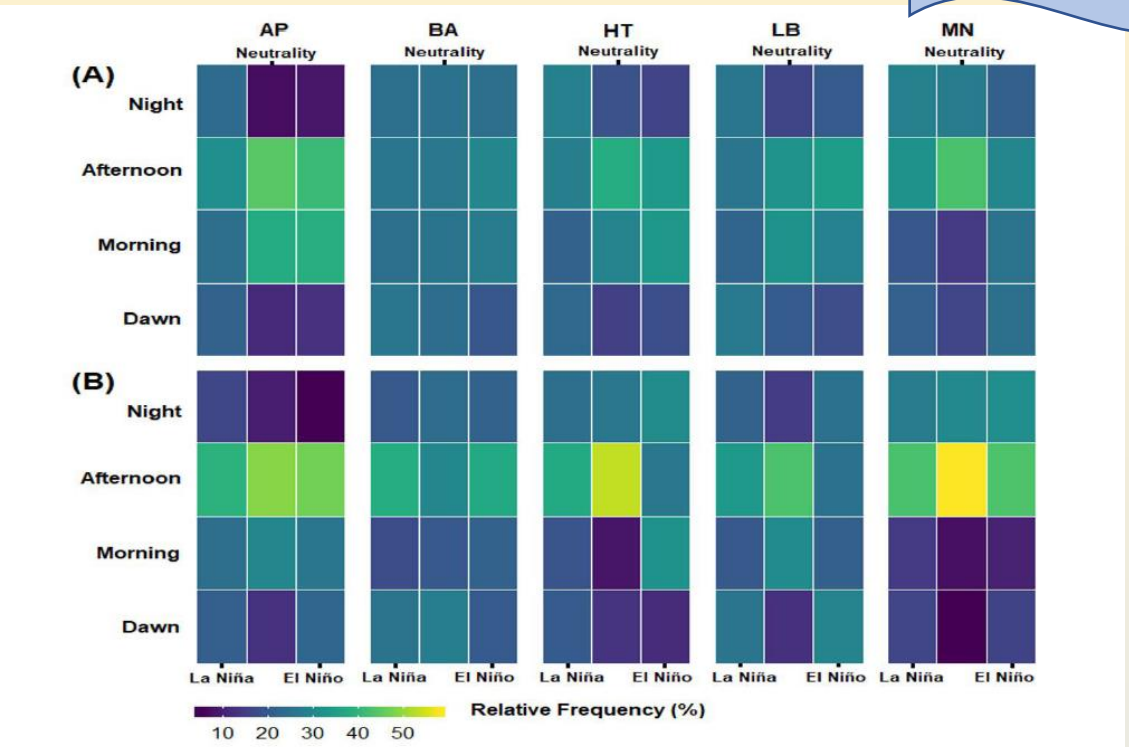

Figure 4. Relative frequency (%) of rainfall on different periods of the day during the wet (A) and dry (B) season in the La Niña (January 1st, 2000 to December 31st, 2000), Neutrality (January 1st, 2013 to December 31st, 2013) and El Niño (January 1st, 2015 to December 31st, 2015) in Apuí (AP), Boca do Acre (BA), Humaitá (HT), Lábrea (LB) and Manicoré (MN).

Description

Pedreira Junior et al. (2020) provides another informative and creative graphical representation of precipitation data acquired from Giovanni. This remarkable figure depicts three different El Niño – Southern Oscillation (ENSO) states (El Niño, La Niña, and neutral**),** two different seasons (wet and dry)**,** five different regions, and four daily divisions to display where and when rain falls in the Amazonas region of South America.

Citation

Pedreira Junior, A.L., Querino, C.A.S., Biudes, M.S., Machado, N.G., Santos, L.O.F.D., and Ivo, I.O. (2020) **Influence of El Niño and La Niña phenomena on seasonality of the relative frequency of rainfall in southern Amazonas mesoregion.** *Brazilian Journal of Water Resources*, 25(24), doi:10.1590/2318-0331.252020190152.

The 2022 Giovanni Image Hall of Fame

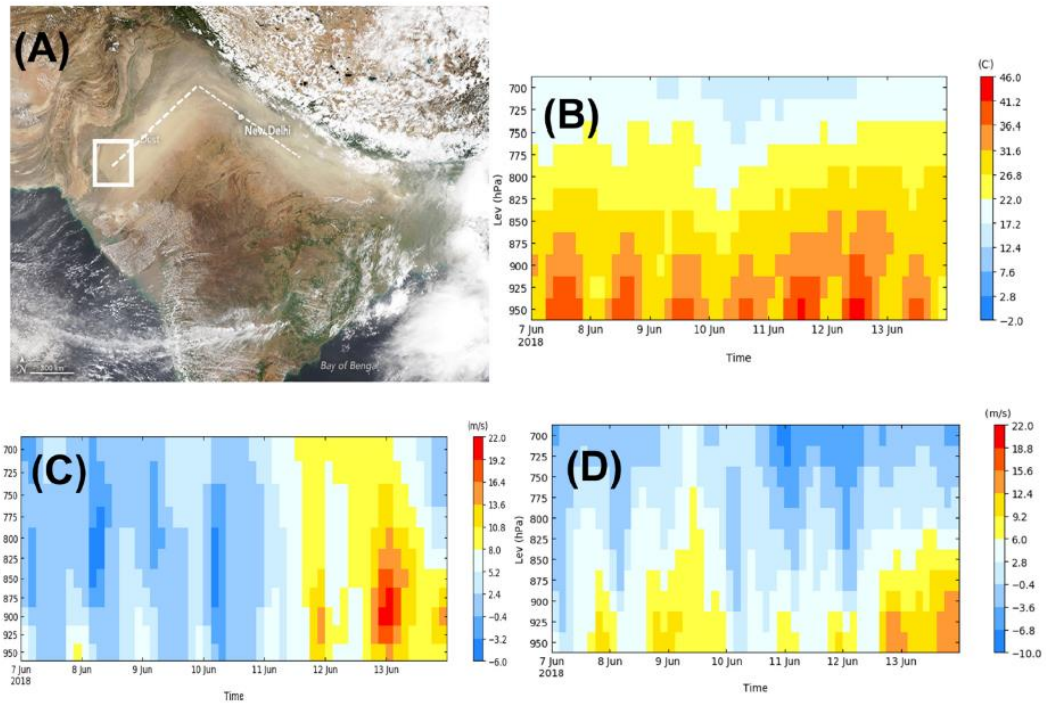

Fig. 1. (A) Reflectance image of MODIS –Terra illustrating the expansion of the dust storm originated from the West Indian region (THAR Desert). The source region is shown by the rectangular box and white dotted line shows the direction of dust transport from the source region. (B) Vertical cross section of the air tmperature (in °C) based on MERRA-2 reanalysis data over the source region. X- axis shows the temporal evolution of the air temperature and Y-axis shows various pressure levels in hPa, colorbar indicates temperature variation in °C (C) same as (B) but for the East-ward wind component (in m/s). (D) same as (B) but for the North-ward wind component (in m/s). Reflectance image has been taken from https://worldview.earthdata.nasa.gov/ and visualisation shown in the (B), (C) and (D) are generated using https://giovanni.gsfc.nasa.gov/.

Description

Singh et al. (2020) effectively used Giovanni's pressure vs. time cross-section plot option in their simulation of a strong dust storm event in India originating from the Thar desert. The true-color image of the dust storm is shown accompanied by pressure vs. time plots of MERRA-2 temperature and both the eastward and northward wind components. The event occurred in the early days of June 2018.

Citation

Singh, C., Singh, S.K., Chauhan, P. and Budakoti, S. (2020) **Simulation of an extreme dust episode using WRF-CHEM based on optimal ensemble approach**. *Atmospheric Research*, 249, 18 pages, doi:10.1016/j.atmosres.2020.105296.

The 2022 Giovanni Image Hall of Fame

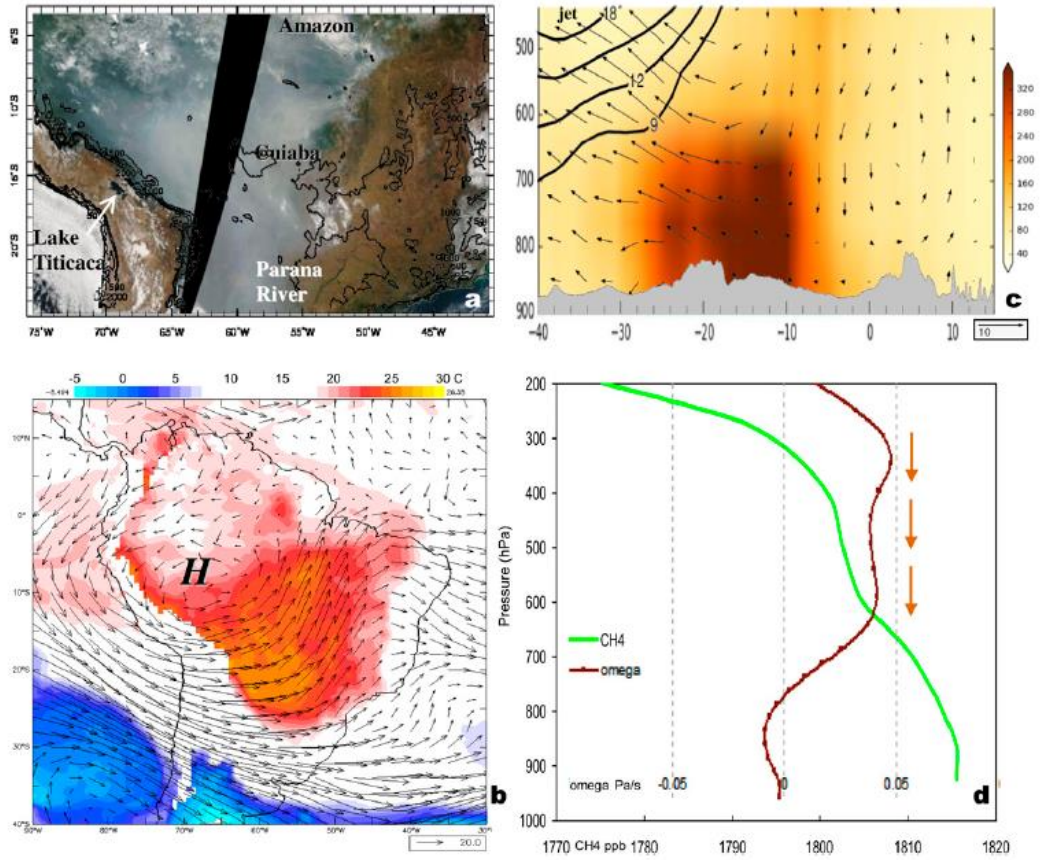

FIG. 8. Maps for 14 Sep 2007 of (a) a MODIS visible image of the smoke plume with topographic details and (b) MERRA-2 near-surface 850-hPa temperature (shaded) and upper 200-hPa winds (vectors). Also shown are mean September 2007 conditions: (c) south–north section 55°–65°W of MOPITT CO (ppb) and NCEP2 meridional circulation vectors and upper-jet contours and (d) profiles of MERRA-2 vertical motion (red, labeled omega; $Pa\,s^{-1}$) and AIRS CH4 concentration (ppb; green). Positive omega refers to sinking motions (as indicated by the arrows).

Description

Satellites have observed extensive wildfires in the rainforest regions of South America for many years. Jury and Gaviria Pabón (2021) examined the meteorological and atmospheric chemistry aspects of wildfire smoke dispersion, using MERRA-2 temperature and wind parameters, carbon monoxide (CO) concentration from the Measurement of Pollution in the Troposphere (MOPITT) instrument, and methane (CH_4) concentrations from the Atmospheric Infrared Sounder (AIRS). Data and plots were acquired from Giovanni. Their figure demonstrates how Giovanni enables the usage of multiple data variables to analyze a topic of interest.

Citation

Jury, M.R., and Gaviria Pabón, A.R. (2021) **Dispersion of smoke plumes over South America**. *Earth Interactions*, 25(1), 14 pages, doi:10.1175/EI-D-20-0004.1.

The 2022 Giovanni Image Hall of Fame

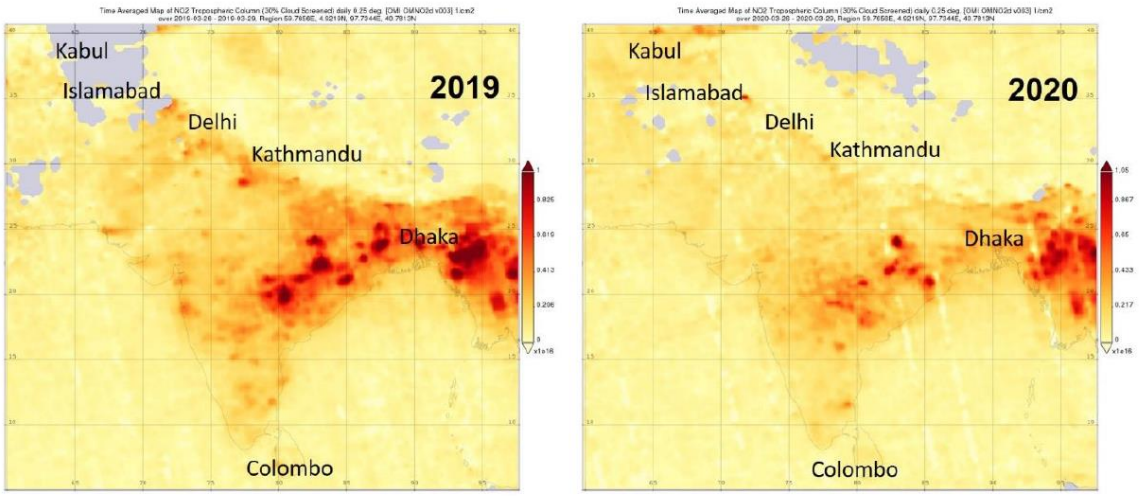

Fig. 1. NO_2 column (from the surface to the top of the tropopause) levels (in mol. cm^{-2}) over South Asia during the last week (25^{th}–31^{st}) of March 2019 and 2020, respectively.

Description

Since the early stages of the COVID-19 pandemic, data from NASA satellites have been key to observing concomitant effects of the attempts of governments to contain and control the outbreak. One strategy to counter the spread of the virus was to drastically reduce commerce and transportation in the forms of societal restrictions and lockdowns. A result of these strategies was temporary and marked improvements in air quality in many heavily-polluted populous regions of the world. A frequently-used tracer of economic activity and transportation is the concentration of nitrogen dioxide (NO_2). Mishra and Kulshrestha (2021) used a Giovanni data map to contrast NO_2 atmospheric concentrations in India and Pakistan for March 2019 and March 2020, clearly showing the reduced concentrations during a lockdown period in March 2020.

Citation

Mishra, M., and Kulshrestha, U.C. (2021) **A brief review on changes in air pollution scenario over South Asia during COVID-19 lockdown**. *Aerosol and Air Quality Research*, 21, 10 pages, doi:10.4209/aaqr.200541.

The 2022 Giovanni Image Hall of Fame

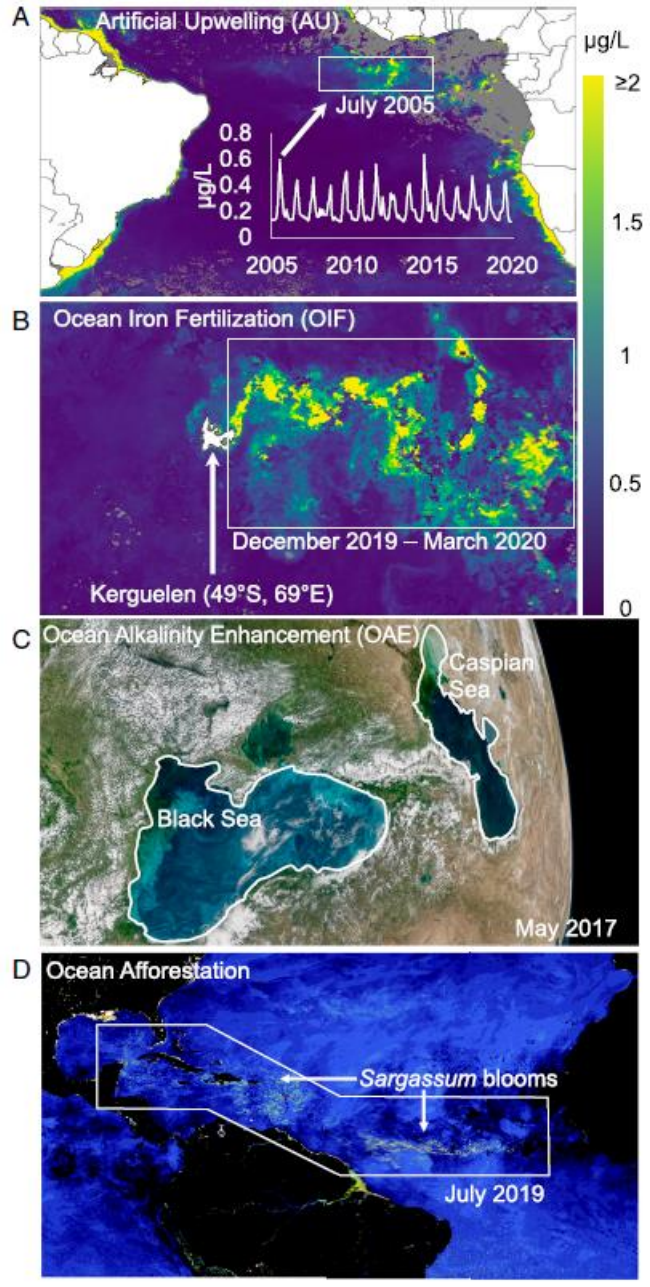

Description

One potential "geoengineering" method of addressing the increasing concentration of carbon dioxide (CO_2) in the atmosphere is adding iron to areas of the ocean where it is the limiting factor for phytoplankton growth. More phytoplankton growth would remove more CO_2 from the atmosphere. As part of an assessment of this technique, Bach and Boyd (2021) looked at natural analogs to this process, where seawater iron concentration is increased by natural processes. Images of phytoplankton chlorophyll concentration from Giovanni were used to show where upwelling transports iron from deeper to shallower oceanic (panels A and B of their Figure 3, shown at left).

Citation

Bach, L.T., and Boyd, P.W. (2021) **Seeking natural analogs to fast-forward the assessment of marine CO_2 removal**. *Proceedings of the National Academy of Sciences*, 118(40), 8 pages, doi:10.1073/pnas.2106147118.

The 2022 Giovanni Image Hall of Fame

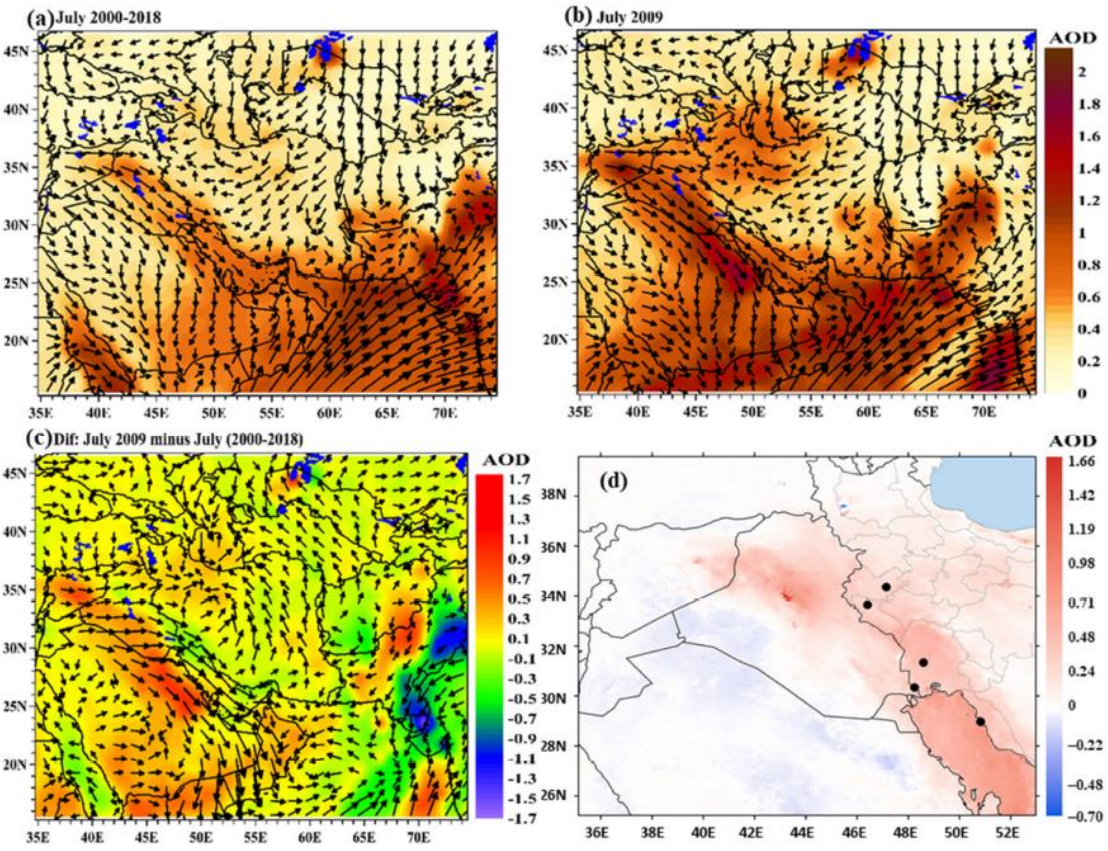

Figure 9. Spatial distribution of Terra-MODIS L3 AOD over the Middle East, south, and central Asia during July 2000–2018 (a), July 2009 (b) and the difference (c). Superimposed vector winds correspond to wind regime over each period and the difference. MODIS level 2 (10 km × 10 km) AOD differences are observed in (d) with an emphasis over the study region. Black dots show the five examined stations in southwest Iran.

Description

Dust and drought are commonly associated with each other. Their connection was the subject of Hamzeh et al. (2021), who examined how dust outbreaks varied over southwestern Iran. They used Giovanni's rapid averaging capability to compare MODIS aerosol optical depth (AOD) averaged for the month of July, (2000-2018) to AOD in July 2019, displayed in panels (a) and (b). The authors created difference maps, panels (c) and (d), for the Middle East and the study region using the data for each time period. They also added vector winds to the Middle East difference map (panel c) to indicate transport direction tendencies.

Citation

Hamzeh, N.H., Kaskaoutis, D.G., Rashki, A., and Mohammadpour, K. (2021) **Long-term variability of dust events in southwestern Iran and its relationship with the drought**. *Atmosphere*, 12(10), 21 pages, doi:10.3390/atmos12101350.

The 2022 Giovanni Image Hall of Fame

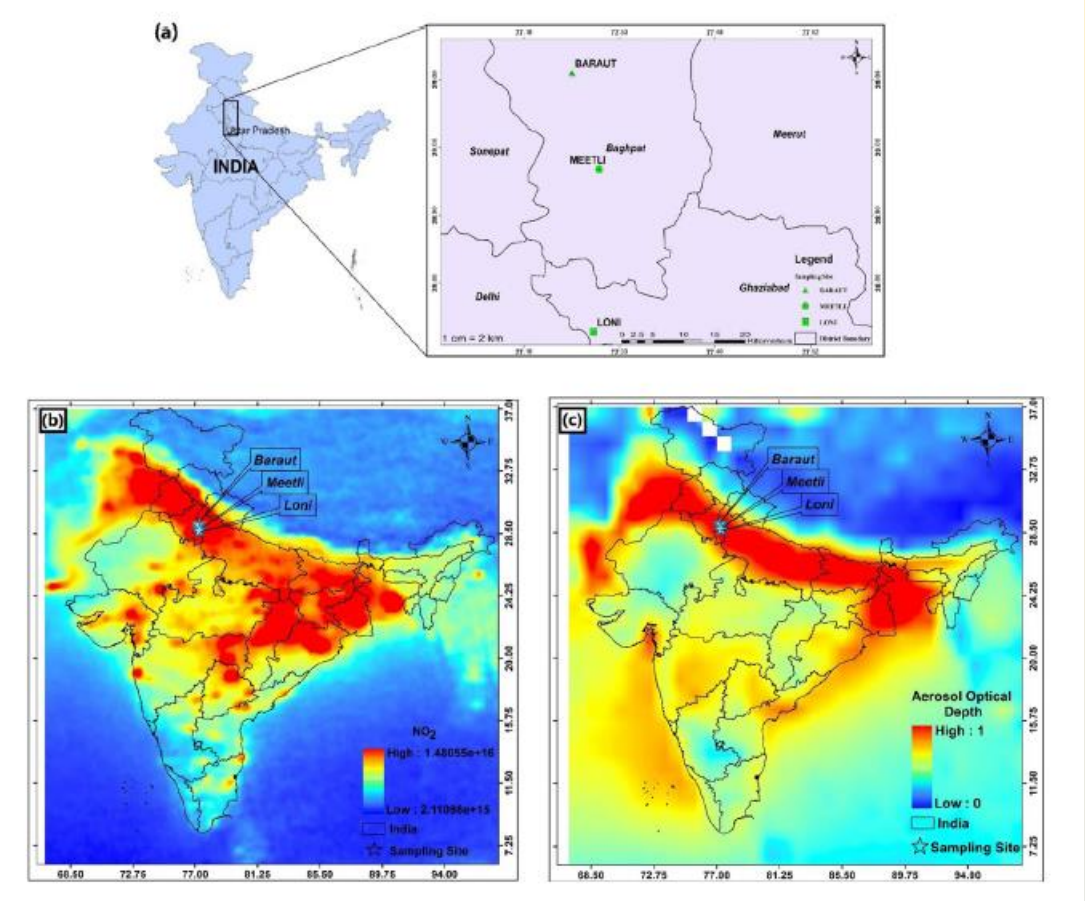

Description

In this paper, the authors investigated the sources and deposition of reactive nitrogen (N), which plays an active role in many important Earth system change processes, including climate, ozone depletion, biodiversity loss, ecosystem acidification, atmospheric aerosol loading, and alteration of the global N cycle. Giovanni was used to plot NO2 and aerosol optical depth across India during the study period of October 2017-September 2018. These plots are shown side-by-side in panels b and c above.

Citation

Naseem, M., and Kulshrestha, U.C. (2021) **Wet deposition of atmospheric inorganic reactive nitrogen (Nr) across an urban-industrial-rural transect of Nr emission hotspot (India).** *Journal of Atmospheric Chemistry*, 34 pages, doi:10.1007/s10874-021-09425-w.

Honorable Mentions

Figure 4 in

Che, H., Gui, K., Xia, X., Wang, Y., Holben, B.N., Goloub, P., Cuevas-Agulló, E., Wang, H., Zheng, Y., Zhao, H. and Zhang, X. (2019) **Large contribution of meteorological factors to inter-decadal changes in regional aerosol optical depth**. *Atmospheric Chemistry and Physics*, 19(16), 10497-10523, doi:10.5194/acp-19-10497-2019.

Figure 1 in

Tangunan, D., Baumann, K.H., and Fink, C. (2020) **Variations in coccolithophore productivity off South Africa over the last 500 kyr**. *Marine Micropaleontology*, 160, 13 pages, doi:10.1016/j.marmicro.2020.101909.

Figure 2 in

Li, M., Shen, F., and Sun, X. (2021) **2019–2020 Australian bushfire air particulate pollution and impact on the South Pacific Ocean**. *Scientific Reports*, 11, 13 pages, doi:10.1038/s41598-021-91547-y.

Figure 3 in

Brumfield, K.D., Usmani, M., Chen, K.M., Gangwar, M., Jutla, A.S., Huq, A., and Colwell, R.R.(2021) **Environmental parameters associated with incidence and transmission of pathogenic *Vibrio* spp**. *Environmental Microbiology*, 28 pages, doi:10.1111/1462-2920.15716.

More Giovanni News !

Coming soon, in the next Giovanni release: Shapefiles for lakes!

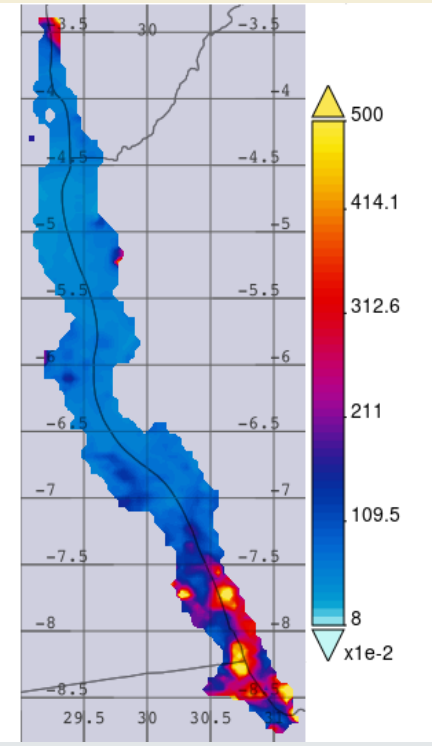

Initiated by a request from members of the Goddard Space Flight Center scientific community and scientists in Africa, the Giovanni development team has been working on adding shapefiles for lakes. In the next release, shapefiles for the world's 125 largest lakes and reservoirs will provide researchers with the ability to examine phenomena and processes in important freshwater resources, particularly those with irregular shapes and which share coastlines with multiple countries. Productivity patterns, turbidity, harmful algal blooms, circulation, weather influences, and changing seasonality are just some of the topics that can be explored with this new visualization capability. The preview at right shows chlorophyll concentrations in Africa's Lake Tanganyika during July 2014.
(Units are milligrams per cubic meter.)